Biol. Cybern. 73, 375–388 (1995)

Biological Cybernetics

Bistability in cerebellar Purkinje cell dendrites modelled with high-threshold calcium and delayed-rectifier potassium channels

G. L. Yuen, P. E. Hockberger, J. C. Houk

Department of Physiology, Northwestern University Medical Center, Chicago, IL 60611, USA

Received: 13 October 1993/Accepted in revised form: 21 March 1995

Abstract. Phase-plane analysis of the ionic currents underlying dendritic plateau potentials was carried out to study the nonlinear dynamics and steady-state transfer properties of the dendritic tree in cerebellar Purkinje cells. The results of an analysis of the P-type calcium and delayed rectifier potassium channel system are presented in this study. These channels constitute a simple system that can support bistability and plateau potentials. By requiring both the steady-state current-voltage curve and nullclines to mimic basic plateau potential properties, we obtained well-defined ranges of specific conductance that can support bistability. Hysteresis was found to be surprisingly prevalent in this simple ion-channel system. Using the steady-state current voltage relationship, we derive concise, algebraic expressions for the voltage and current thresholds of state transitions as functions of specific conductance. The significance of bistability in this ion-channel system is discussed with respect to the generation of plateau potentials in Purkinje cells dendrites and the role of the cerebellum in motor control.

1 Introduction

The analysis of networks comprised of relatively simple models of individual neurons has provided considerable insight into the information processing capabilities of the nervous system (Anderson and Rosenfeld 1988). Single-neuron models that have been widely used include linear threshold or threshold-logic (Minsky and Papert 1969), integrate-and-fire (Knight 1972), sigmoidal (Hopfield and Tank 1986), and others (cf. Rumelhart and McClelland 1986). In some cases, however, these simple models fail to capture what appear to be the essential computational properties of a neuron type. For example, Purkinje cells of the cerebellar cortex have conspicuous nonlinear dynamical properties due to an abundance of voltage-dependent ionic conductances in their dendritic membranes. These features give rise to a form of bistability that is believed to be the origin of important computational properties of the cerebellar cortex (Houk et al. 1990).

The Purkinje cell model shown in Fig. 1A has been used in several recent simulation studies to explore the role of the cerebellum in limb movement control (Houk et al. 1990; Sinkjaer et al. 1991; Houk and Barto 1992; Berthier et al. 1993). While this model displays bistability, it is a simple abstraction of actual Purkinje cell properties without any clear biophysical justification. Several groups have published detailed, multicompartment models of Purkinje cells (Pellinoisz and Llinas 1977; Bush and Sejnowski 1991; de Schutter and Bower 1994). However, these models are fairly complex and contain too many variables to be desirable for the type of large-scale simulations needed in motor control. What we seek in the present work is an intermediate level of description which allows the bistable transfer function in Fig. 1A to be related to the properties of the dominant ionic conductances. It is well-known that Purkinje cells have an asymmetric distribution of voltage-dependent ion channels resulting in predominantly fast sodium conductances in the soma (Llinás and Sugimori, 1980a; Lasser-Ross and Ross 1992), slow calcium conductances in the dendrites (Llinás and Sugimori 1980b; Ross and Werman 1987; Tank et al. 1988; Lev-Ram et al. 1992), and slow potassium conductances in both somatic and dendritic compartments (Llinás and Sugimori 1980a, b; Gähwiler and Llano 1989). These observations suggested to us that the overall response properties of a Purkinje cell might be approached from an analysis of the slower channels in an individual dendrite, followed by an examination of an integrated model comprised of a soma and multiple dendrites.

Here we report on a single-compartment model of a dendrite with high threshold calcium and delayed rectifier potassium conductances, both of which are found in Purkinje cells (Yool et al. 1988; Gähwiler and Llano 1989; Regan 1991; Mintz et al. 1992; Usowicz et al. 1992). High threshold calcium conductances are thought to underlie the 'plateau potentials' recorded from Purkinje

Correspondence to: J. C. Houk

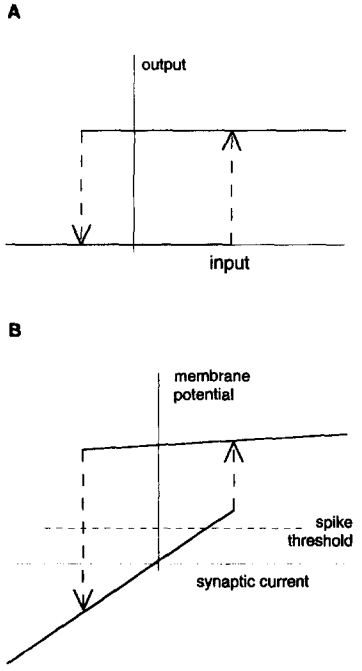

Fig. 1. Contrasting models of bistability in Purkinje cell dendrites: **A** abstract model used in network simulations; **B** ionic model derived from present results, based on the steady-state properties of a dendrite containing high-threshold calcium and delayed-rectifier potassium channels

cell dendrites (Llinás and Sugimori 1980b; Ekerot and Oscarsson 1981; Andersson et al. 1984). Plateau potentials represent a form of bistability in the sense that a brief injection of inward current results in a depolarization that is sustained beyond the duration of the current pulse, and this depolarization can be switched off by the application of a brief outward current pulse. Thus, the dendrite expresses two stable states, which is the definition of bistability. However, the period of bistability is limited in duration as plateau potentials tend to reset after a period of a few hundred milliseconds. This resetting is thought to be due to another type of potassium channel, one that is activated by the accumulation of intracellular calcium. In the present model, we neglect the latter channel in order to concentrate on the basic phenomena of bistability.

In pursuing the goal of simplification, we have adopted the qualitative nonlinear dynamical approach that has been promoted by Fitzhugh, Rinzel and others (Fitzhugh 1959; Morris and Lecar 1981; Rinzel and Ermentrout 1989; Rose and Hindmarsh 1985). Qualitative nonlinear dynamics attempts to capture the essential characteristics of a complex system within the framework of a low-order, typically second-order, nonlinear dynamical model. After reducing the system to second order with only two state variables, the stability properties and response trajectories of the model can be visualized in a two-dimensional phase plane. These plots provide a qualitative, geometric view of how dynamic trajectories relate to the stable and unstable equilibrium points of the system, thus allowing prediction and classification of the various system responses.

By studying the phase portrait and steady-state current-voltage relationship simultaneously and by constraining the model to mimic certain properties of plateau potentials, we have been able to relate the transfer function in Fig. 1A to specific biophysical (channel conductance) parameters. These results therefore provide a means for comparing hypothetical and biological bistable transfer functions. Some of the pilot results from this study have been reported previously (Yuen et al. 1992).

2 Dendritic model

Several types of voltage-dependent calcium and potassium conductances are present in Purkinje cells. This paper will focus on the interaction between two of them, high-threshold calcium and delayed rectifier potassium. These two conductances support bistability in barnacle muscle cells (Morris and Lecar 1981) and were chosen to facilitate comparisons to be made with the bistable, hysteretic transfer function in Fig. 1A. A Hodgkin and Huxley type of model for this system can be described by three differential equations,

$$C_m \frac{dV}{dt} = -(I_{Ca} + I_K + I_{leak}) + I_{inj} \tag{1}$$

$$\frac{dn}{dt} = \frac{n_{inf} - n}{\tau_n} \tag{2}$$

$$\frac{ds}{dt} = \frac{s_{inf} - s}{\tau_s} \tag{3}$$

Equation (1) expresses the fact that changes in membrane voltage are proportional to the sum of the ionic and injected currents, where the membrane capacitance C_m is the constant of proportionality. Equations (2) and (3) describe the dynamics of the gate opening variables for potassium channels, n, and for calcium channels, s. In both cases, the rate of gate opening is proportional to the difference between the steady-state values of the gating variables (n_{inf} and s_{inf}) and their instantaneous values. The gating variables take on values between 0 and 1.

The potassium and calcium currents on the right-hand side of (1) can be expressed as the product of the maximum conductance value, the gate opening variable raised to an appropriate power, and the electrochemical driving force:

$$I_K = g_K n^4 (V - V_K)$$

$$I_{Ca} = g_{Ca} s^2 (V - V_{Ca})$$

where g_K is the maximum conductance for potassium, n is the instantaneous gate-opening of the potassium channels, V is the transmembrane potential, and V_K is the potassium equilibrium potential. The terms for the high-threshold calcium current are similarly defined. The leakage current has a constant conductance g_{leak}.

$$I_{leak} = g_{leak} (V - V_{leak})$$

The steady-state values of the gating variables vary with the membrane potential V. These activation functions, $n_{inf}(V)$ and $s_{inf}(V)$, were obtained by fitting data obtained from rat Purkinje cells under voltage-clamp conditions (Hockberger and Nam 1994; Hockberger, unpublished data). These data were normalized and fitted to the Boltzman equation,

$$f = \frac{1}{1 + \exp((V + V_{half})/k)}$$

where f varies sigmoidally from 0 to 1 and represents the extent of activation of the channel as a function of V. The constants V_{half} and k are the half-maximum voltage and slope of the sigmoid, respectively. The former defines the voltage at which the channel is half activated, while the latter describes the slope of the sigmoid curve at V_{half}. The argument of the exponential function in f is unitless and thus V, V_{half}, and k all have units of 'mV'. The following values for high threshold calcium and delayed rectifier potassium channels, i.e., for s_{inf} and n_{inf}, were used in the simulations and analysis: $[V_{half}, k] = [17.8\ \text{mV},\ 4.53\ \text{mV}]$ and $[10.5\ \text{mV},\ 11.5\ \text{mV}]$, respectively.

Similarly, the voltage dependence of the time constant of delayed rectifier potassium and high threshold calcium activation was based on the same data which were fitted empirically to the following function,

$$\tau_n = \frac{A}{\exp\left(\frac{V + V_{max}}{k}\right) + \exp\left(\frac{V + V_{max}}{k}\right)} + B$$

where $A = 4.0$ ms, $B = 0.4$ ms, $V_{max} = 7.5$ mV, and $k = 17.5$ mV. Graphically, V_{max} corresponds to the peak of the time constant curve on the voltage axis, A is the maximum value of the time constant, and B is the steady time constant value at very depolarized or hyperpolarized voltages (assumed to be equal). Analogously, the kinetics for the delayed rectifier potassium channels are described by $A = 4.15$ ms, $B = 0.2$ ms, $V_{max} = -22.5$ mV, and $k = 17$ mV. No inactivation processes are included here as they have slower time constants than the plateau potentials.

In initial simulations, standard Hodgkin and Huxley type 'rate functions' (i.e. alphas and betas) were used to compute activation and time constants (Hodgkin and Huxley 1952). However, these expressions contained singularities which led to invalid deviations from the theoretical steady-state current-voltage properties. To obtain a close correspondance between the numerical integration and theoretical results, we abandoned the original mathematical form of the rate functions (the alphas and betas) and adopted the expressions as shown above to describe the activation and kinetics. These smooth functions concurrently allowed Gear's method for numerical integration to be used, which is very efficient for stiff systems such as Hodgkin-Huxley type of differential equations (Mascagni 1989). Gear's method is based on the Adams linear-multistep method with explicit prediction and implicit correction (Gear 1971). For the problem at hand, Gear's method reduced the computational time by about 45% compared with the fourth-order variable time-step Runge-Kutta method.

The dendrite was modeled by a single electronic compartment (cf. Llano et al. 1991). Shelton (1985) has estimated the total surface area of Purkinje cells to be 120 000 mm^2, and we assumed that dendrites account for 97% of this. We used $C_m = 1\ \mu\text{F/cm}^2$ and $R_m = 50\,000\ \Omega\,\text{cm}^2$, yielding a passive time constant of 50 ms; g_{leak} was $1/R_m = 20\ \mu\text{S/cm}^2$, and V_{leak} was set to -60 mV. The interaction between I_{leak} and resting I_K gave rise to a resting membrane potential of -68 mV, within the range observed in recent recordings that employed high-impedance microelectrodes (Larson-Prior et al. 1990). V_{Ca} was assumed to be $+80$ mV, and g_{Ca} was varied about a default value of $60\ \mu\text{S/cm}^2$ (see Discussion). V_K was assumed to be -85 mV, and g_K was varied about a default value of $420\ \mu\text{S/cm}^2$ (see Discussion). The default values were chosen to obtain plateau potentials with reasonable properties, as elaborated later.

Comparing the simulated responses for the third-order model (1)–(3) and a second-order model obtained by assuming $ds/dt = 0$ revealed that the two models have virtually identical trajectories except for the threshold voltage for switching states, where the models differed by only 1 mV. Therefore, we restricted our attention to the second-order model, ignoring the kinetics of the calcium channel so that

$$I_{Ca} = g_{Ca}s^2(V - V_{Ca}) \cong g_{Ca}s_{inf}^2(V - V_{Ca})$$

Thus, the single-compartment dendritic model described below has just two state variables: membrane voltage (V) and potassium channel activation (n).

3 Phase-plane analysis

The nonlinear dynamics of the second-order dendritic model defined in the previous section can be analyzed as trajectories on a phase plane in which the two state variables, n and V, serve as coordinates. The phase trajectories will intersect the system's nullclines at specified slopes as they converge toward equilibrium points that are defined by the intersections of the nullclines (Rinzel and Ermentrout 1989). Thus, a first step in the analysis is to compute and plot the two system nullclines. Each nullcline is defined by setting the time derivative of one of the state variables to zero. The resultant function can then be plotted on the phase plane to indicate the locus of points where one of the state variables is not changing as a function of time. Setting $dV/dt = 0$ in (1), substituting the expression for I_K, and then solving for n in terms of V, one obtains the voltage nullcline:

$$n = \left[\frac{-(I_{Ca} + I_{leak} - I_{inj})}{g_K(V - V_K)}\right]^{1/4} \tag{4}$$

I_{Ca} and I_{leak} are functions of V given earlier. The potassium nullcline is obtained by setting $dn/dt = 0$ in (2) and

A

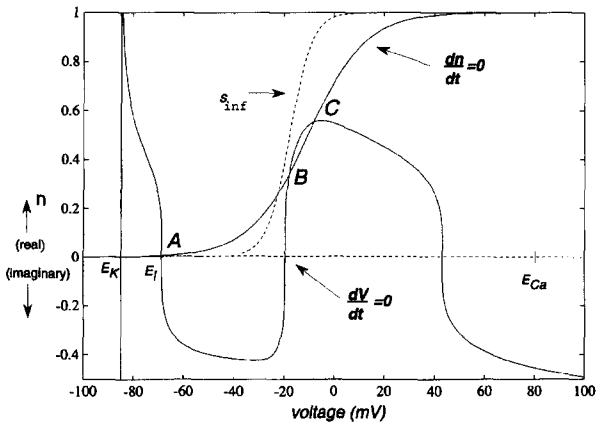

B

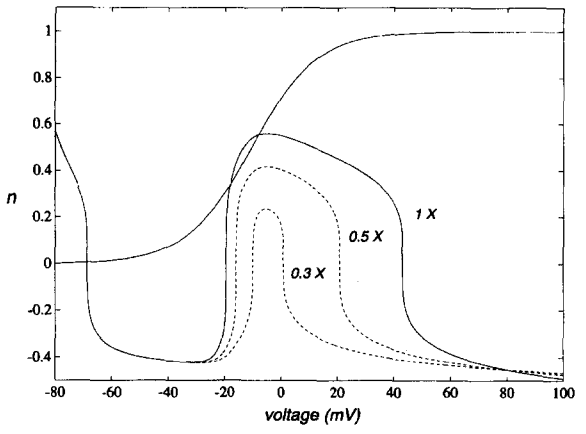

Fig. 2A, B. System nullclines and equilibrium points. **A** *Solid lines* show the nullclines obtained when standard values of g_{Ca} (60 μS/cm^2) and g_K (420 μS/cm^2) are used. The potassium nullcline is the sigmoidal curve obtained by setting $dn/dt = 0$, reflecting the voltage-dependence of the potassium conductance. The voltage nullcline is the complex curve obtained by setting $dV/dt = 0$, reflecting properties of the full set of conductances. The intersections at points *A*, *B*, and *C* are the equilibrium points of the system. The *dashed curve* s_{inf} is the steady-state voltage dependence of the calcium conductance. **B** Modifications (*dashed curves*) in the voltage nullcline resulting from decreasing the specific conductance assumed for calcium eliminate the upper two equilibrium points. Plateau potentials are not possible under these conditions

substituting the Boltzman expression for $n_{inf}(V)$:

$$n = n_{inf} = \frac{1}{1 + \exp((V + V_{half})/k)} \tag{5}$$

In Fig. 2A, the solid sigmoidal curve corresponds to the nullcline for the potassium gating variable n (4), while the tilted S-shaped curve corresponds to the voltage nullcline (3). The complex shape of the voltage nullcline is a result of the leakage conductance (which affects the region near the resting membrane potential), the potassium conductance (which causes n to assume unrealizable imaginary values), and the calcium conductance (which contributes to the 'hump' between -20 and 40 mV). The dependence of this hump on the calcium current is illustrated in Fig. 2B where it is shown that the hump is progressively attenuated by reducing the magnitude of calcium conductivity g_{Ca}. The shape of s_{inf} is shown dashed in Fig. 2A for comparison with n_{inf}; as the dendritic membrane depolarizes, potassium channels activate at lower depolarizations and calcium channels at higher depolarizations. This is why the voltage nullcline dips downward before the hump.

The equilibrium points of the system are marked by the intersections of the two nullclines, since at these points dV/dt and dn/dt are both equal to zero, meaning that the system state is unchanging. In order for the system to express bistability, there must be three equilibrium points, as illustrated by A, B, and C in Fig. 2A. A local stability analysis (Rinzel and Ermentrout 1989) indicated that A and C are stable points, having only negative eigenvalues, while B has one positive eigenvalue and therefore is unstable. Figure 2B shows that attenuating the calcium conductance alters the system to one with a single equilibrium point, the resting potential of the dendrite. This demonstrates that the existence of bistability requires a certain density of calcium channels, which translates into the assumed value for the maximal calcium conductivity, g_{Ca}. Other features constrain the value of g_K. Conductivities of 60 and 420 μS/cm^2 for calcium and potassium provided suitable bistable properties and thus were used in constructing the examples illustrated in Figs. 2–4. The manner in which system properties depend on channel conductivities is fully analyzed in later sections of this paper.

The phase portrait shown in Fig. 3A is completed by plotting a family of phase trajectories to illustrate how system state (V and n) evolves with time, starting from various initial states. Regardless of the choice of initial condition, the system state eventually converges onto one of the two stable points, *A* or *C*, along the trajectories marked by the arrowheads. If we plot a phase trajectory starting from a point below the voltage nullcline, $dV/dt > 0$, and voltage will tend to increase over time. For initial conditions above the voltage nullcline, $dV/dt < 0$, and V will decrease over time. Trajectory intersections with the voltage nullcline are vertical lines since $dV/dt = 0$. Analogously, n values increase to the right of the potassium nullcline ($dn/dt > 0$) and decrease to the left ($dn/dt < 0$). Trajectory intersections with the potassium nullcline are horizontal lines since $dn/dt = 0$. These rules allow one to sketch trajectories without solving the differential equations; however, the trajectories plotted in Fig. 3A are actually simulations. The portion of the voltage nullcline with imaginary values of n is unrealizable, and simulations never entered this region.

Initial states at *a*, *b*, and *e* in Fig. 3A illustrate typical subthreshold passive responses, while *c* and *d* reflect suprathreshold active responses. Since the middle intersection of the nullclines at *B* is a saddle point, trajectories always diverge from this intersection. The presence of the saddle point creates a locus of thresholds between the passive off-state of the system, where calcium and potassium channels are essentially closed, and the active

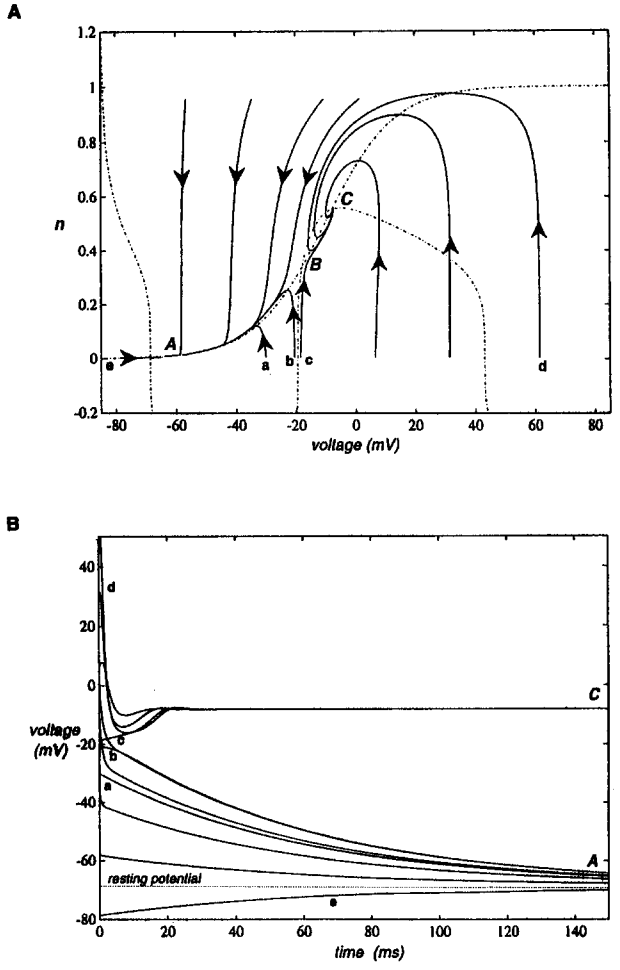

Fig. 3A, B. Family of transient responses generated by starting from several initial states (*a–e*). **A** *Solid curves with arrows* show the transients as phase trajectories. Subthreshold initial states return system to the lower equilibrium point *A* (*a, b, e*), while suprathreshold initial states launch system to its excited equilibrium point *C* (*c, d*). *B* is an unstable equilibrium point (a saddle point) from which the trajectories diverge. **B** The same family of transients shown as functions of time. Note that transients to the excited state *C* are more rapid than those that converge upon the resting state *A*. Standard values of g_{Ca} (60 μS/cm^2) and g_K (420 μS/cm^2) were used

on-state, where both of these channels are relatively open. The trajectories tend to run parallel to the *n*-axis due to the slow passive response of the electrotonic time constant (50 ms).

The corresponding system responses in the time domain are shown in Fig. 3B. Note how these transients follow a time course that varies depending on the initial state of the system, this feature being an expression of the system's nonlinearity. Subthreshold initial conditions (such as *a*, *b* or *e*) lead to slow repolarization to the resting potential at equilibrium point *A*, while suprathreshold initial conditions (such as *c* and *d*) stabilize more rapidly to equilibrium point *C*. In theory, the membrane potential could remain indefinitely in the depolarized on-state at point *C*. Alternatively, an external event could provoke a transition that would return it to the resting state at point *A*.

4 Bistable current-voltage relationships

The transitions between off- and on-states mentioned in the previous section would ordinarily be induced by changes in excitatory and inhibitory synaptic current. Excitatory current would produce transitions to the on-state, whereas inhibitory current would produce transitions to the off-state. In the present model, we simulated the effects of synaptic current by altering $I_{injected}$ in (1). Figure 4A shows responses to brief pulses of current with amplitudes near the threshold for state transitions. When the amplitude of the pulse was just below threshold, the membrane potential charged to a depolarized value during the pulse and discharged back to resting potential after the pulse ended. However, a pulse of slightly greater amplitude caused an upward inflection in membrane potential during the pulse, and the membrane latched into a depolarized state that continued after the pulse ended. This latter response simulates a plateau potential. The plateau was terminated (reset to the off-state) by a subsequent negative current pulse simulating synaptic inhibition.

Figure 4B shows responses of the same dendritic model to step changes of current. The steps simulate steady-state responses to sustained excitatory synaptic inputs. As with the pulses, a marked jump in voltage occurred when the amplitude of the current exceeded a certain critical value. Above this value, which we will call the on-threshold of the membrane, there was an abrupt jump in voltage resulting in a transition to the on-state. The threshold for an on-transition was 0.89 nA for steady current stimuli. This threshold was somewhat higher for the pulse stimuli (about 1.4 nA), due to the filtering effect of the membrane time constant. Regardless of this, the resultant state transition was clearly an expression of bistability, since the membrane remained in the depolarized state after the stimulating current was removed (not explicitly shown in Fig. 4B).

One can analyze these state transitions by plotting the alterations in the voltage nullcline that are caused by different amplitudes of steady injected current. The dashed curves above the solid voltage nullcline in Fig. 4C show how positive currents progressively attenuate the dip in the voltage nullcline, while also slightly elevating the peak of the hump. Small positive currents shift the lower intersection point in a depolarizing direction, illustrated as a shift from *A* to *A'* in Fig. 4C. This accounts for the graded membrane depolarizations illustrated by the lower three traces in Fig. 4B. Larger currents do something qualitatively different – they substantially attenuate the dip which removes two of the three intersections in Fig. 4C. Membrane potential must then jump to the only remaining equilibrium point, *C'*, for the example, in which the injected current is 1.2 nA. This qualitative change in phase-plane intersections explains why the upper voltage traces in Fig. 4B jumped up to a plateau (at approximately -8 mV). If the injected current is returned to zero, the membrane potential falls slightly, but the membrane remains in its depolarized on-state, as characterized by equilibrium point *C* in Fig. 4C. This is another way of illustrating the membrane's bistability.

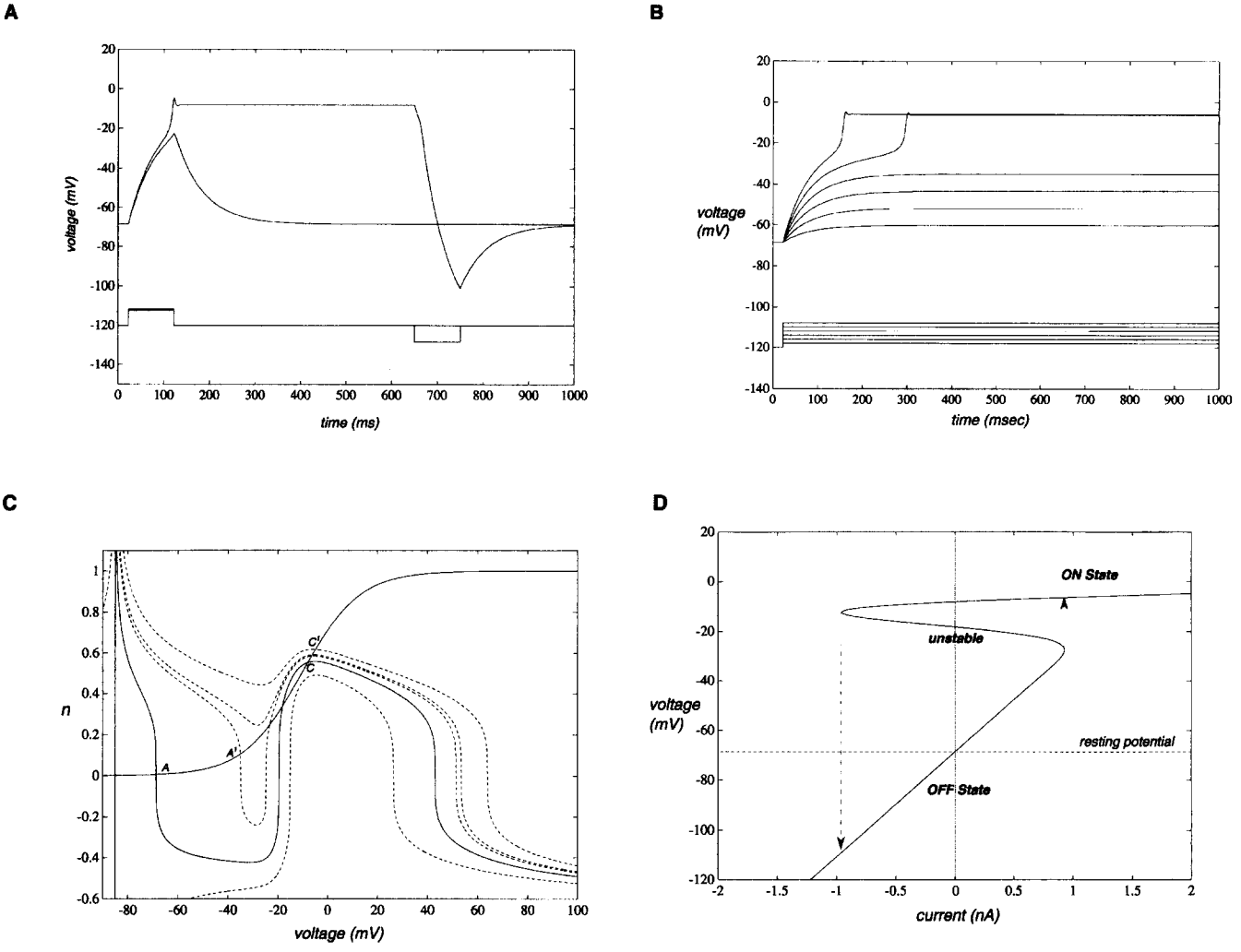

Fig. 4A–D. Membrane potential responses to injected currents. **A** Responses to brief (100 ms) pulses mimicking transient synaptic input illustrate the sharp threshold for transitions to the on-state. The response to a 1.3-nA pulse returns to resting potential, whereas a 1.4-nA pulse produces a transition to the on-state followed by a plateau potential. The plateau is reset to resting potential by a brief hyperpolarizing pulse (1.4 nA). **B** Responses to steps of current mimic steady-state responses to sustained synaptic input. The injected current amplitude ranges from 0.2 nA (lowest trace) to 1.2 nA (uppermost trace) in 0.2-nA increments. Steady current 1 nA produces a transition to the on-state. **C** A phase-plane analysis of the effects of steady current injection reveals changes in system equilibrium points. The *solid* voltage nullcline corresponds to an absence of injected current. Depolarizing current attenuates the dip and shifts the nullcline upward; 0.8 nA of injected current moves the resting equilibrium point from A (resting membrane potential) to a more depolarized value (A'); 1.0 and 1.2 nA eliminate the lower equilibrium points, forcing a shift to the on-state (C'). Removal of the injected current would leave the system in its on-state at point **C**. Hyperpolarizing current accentuates the dip and shifts the voltage nullcline downward; -1.6 nA eliminates the upper equilibrium points forcing a shift back to the off-state (off the graph to the left). **D** The steady-state relation between injected current and membrane potential displays bistability. In the lower stable region, the off-state, the membrane follows the passive resistance of the membrane. In the upper stable region, the on-state, membrane resistance is low because calcium and potassium conductances are activated. An intermediate unstable state defines a region of hysteresis. The *dashed lines* illustrate on- and off-thresholds for state transitions. Standard values of g_{Ca} (60 μS/cm^2) and g_K (420 μS/cm^2) were used

Just as positive currents of sufficient amplitude produce transitions from the off- to the on-state, negative currents of sufficient amplitude produce transitions from the on- back to the off-state. The way in which this works can be appreciated from the lowest dashed curve in Fig. 4C. This is the nullcline in the presence of a steady negative current. Negative current accentuates the dip in the voltage nullcline, while also counteracting the hump. Sufficient current moves the hump below the potassium nullcline, which eliminates two of the intersections marking equilibrium points. Although not shown in Fig. 4C, this value of negative current moves the lowest equilibrium point leftward from A to an intersection at approximately -130 mV. Because the upper intersection is eliminated, the membrane jumps into this passive off-state, closing the calcium and potassium gates. Now when the negative current is removed, the membrane goes back to its resting state at intersection A. The steady-state relationship between voltage and injected current can be derived analytically by setting the time derivatives of the state variables to zero in (1) and (2) ($dn/dt = dV/dt = 0$), and rearranging

to yield

$$n = n_{\text{inf}} \tag{6}$$

$$I_{\text{inj}} = \sum I_{\text{ions}} = I_{\text{Ca}} + I_{\text{K}} + I_{\text{leak}} \tag{7}$$

Using (4) to obtain a steady-state expression for I_{K} and substituting this along with steady-state expressions for the other ionic currents into (5), one then obtains an expression for the value of injected current that corresponds to each steady-state voltage, in analogy with a voltage-clamp experiment. The resultant current-voltage relationship, which is plotted in Fig. 4D, has two stable ranges characterized by positive resistance (slope of the current-voltage curve) separated by an unstable region where the equivalent resistance of the dendrite assumes a negative value. The latter region can only be explored under voltage-clamp conditions. Otherwise, when currents exceed the on-threshold (in this case 0.89 nA), the voltage skips over the unstable region, jumping vertically to the on-state region. After this transition, the dendrite will remain in on-state even if the current is reduced to zero. It will return to the off-state only if a negative current that exceeds an off-threshold (in this case -0.92 nA) is injected. The existence of the unstable negative slope region guarantees that the dendrite will behave in a bistable manner over the range of injected currents corresponding to the negative slope region.

5 Dependence of hysteresis on specific conductances

It is apparent from the results presented in the previous section that the response of this dendritic model depends not only on the prevailing input but also on the past history of its input, which amounts to a type of short-term memory. This kind of nonlinearity with memory in the system response is called hysteresis. The properties of the hysteretic region of the current-voltage relationship are critically dependent on the specific conductances assumed for calcium and potassium ion channels. Figure 5A shows that increasing the calcium conductance substantially widens the hysteresis region by increasing the magnitude of the off-threshold current while only slightly decreasing the on-threshold current. Since it is unrealistic to expect (inhibitory) synaptic currents larger than about 20 nA, one can use the width of the hysteresis region as a constraint on calcium conductance. Increasing potassium conductance has an opposite and less dramatic effect; it diminishes the hysteresis region. In addition to altering the width of the hysteresis region, increases of either calcium or potassium conductance decrease the input resistance of the dendrite when it is in the on-state.

With a three fold increase in g_{K}, the off-threshold actually crosses the origin of the abcissa (Fig. 5A), such that bistability no longer exists, unless a steady depolarizing current is present. This situation is illustrated more clearly in Fig. 5B where, for these values of g_{Ca} and g_{K}, the hysteretic region occurs between $+0.25$ and $+0.95$ nA. The dendrite might operate around this more

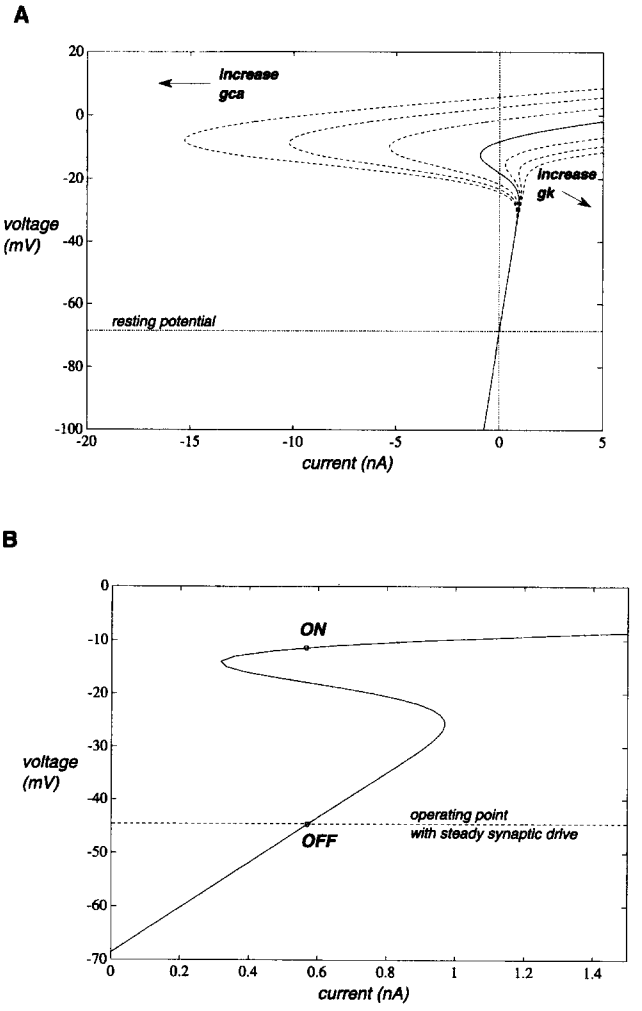

Fig. 5A, B. Effect of specific conductances on the current-voltage relation. **A** Increasing g_{Ca} substantially widens the hysteresis region of the current-voltage relation by increasing the magnitude of the off-threshold. The *control curve* was obtained with standard values of g_{Ca} (60 μS/cm^2) and g_{K} (420 μS/cm^2), whereas the *dashed curves to the left* correspond to a g_{Ca} of 240, 180, 120 mS/cm^2, maintaining $g_{\text{K}} = 420$ mS/cm^2. Increasing g_{K} decreases the region of hysteresis. The *dashed curves to the right* correspond to a g_{K} of 840, 1260, 1680 mS/cm^2, maintaining $g_{\text{Ca}} = 60$ μS/cm^2. **B** With a threefold increase in g_{K}, the off-threshold crosses the origin of the current axis. Bistability then exists only in the presence of a depolarized operating point, as might be produced by a steady synaptic drive. A short current pulse (0.8 nA, 100 ms) then sends the system to the on-state (*upper open circle*). Calcium and potassium conductivities: 39 and 420 mS/cm^2, respectively

depolarized resting potential under the influence of a steady synaptic excitatory current, which might arise from parallel fiber background activity (Rapp et al. 1992). A short depolarizing input superimposed on the steady synaptic background would then switch the system to the on-state illustrated in Fig. 5B.

The dependence of hysteresis on specific conductances can be investigated by determining how on- and off-state transitions are influenced by the conductances. An analytic expression for the locus of state transitions can be found by taking the derivative of the current-voltage relationship (5). This is because $\mathrm{d}I/\mathrm{d}V$ goes

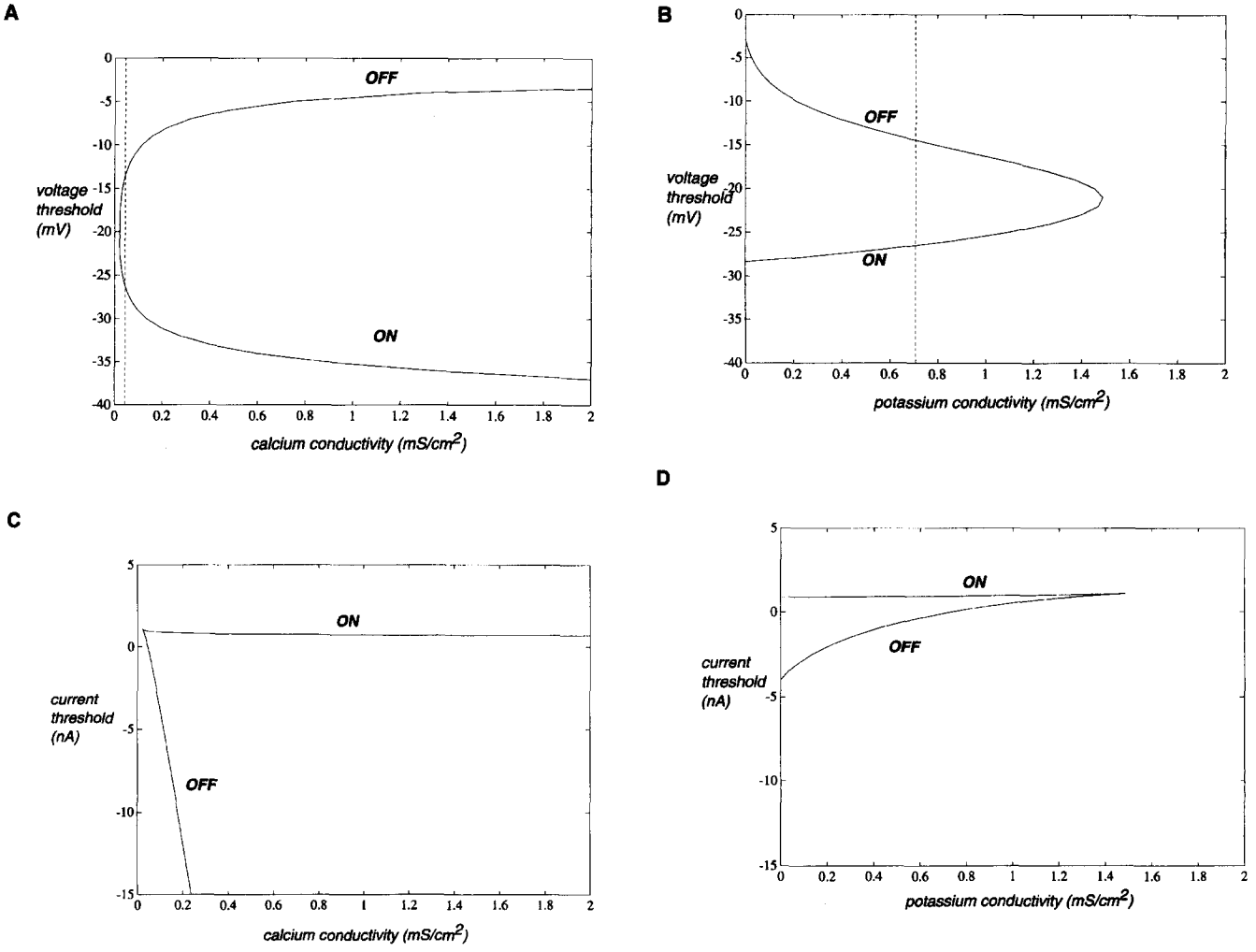

Fig. 6A–D. Effect of specific conductances on voltage and current thresholds for state transitions. Voltage (**A**) and current (**C**) thresholds are shown as a function of calcium conductance when potassium conductance is held at its standard value (0.42 mS/cm^2). Voltage (**B**) and current (**D**) thresholds are shown as a function of potassium conductance when calcium conductance is held at its standard value (0.06 mS/cm^2). The *vertical dashed lines* in **A** and **B** correspond to the condition in which the off-threshold occurs at zero injected current. At lower values of g_{Ca} and higher values of g_K, bistability only occurs in the presence of steady depolarizing current

through zero (dV/dI becomes infinite) at the on- and off-thresholds, due to inflections in the current-voltage curve (Fig. 4D). In the Appendix, we use this feature to derive expressions showing how voltage and current thresholds depend on the specific conductances of calcium and potassium channels; these expressions are plotted in Fig. 6. Figure 6A shows the dependence of the voltage on- and off-thresholds on calcium channel specific conductance when potassium channel conductance is held fixed at 420 μS/cm^2, corresponding with the standard value used for g_K in earlier illustrations. Similarly, Fig. 6B shows voltage thresholds as a function of potassium channel conductance when calcium channel conductance is held fixed at 60 μS/cm^2, corresponding with the standard value used for g_{Ca}. The zones between on- and off-thresholds show how the regions of hysteresis expand with higher calcium channel densities and contract with higher potassium channel densities. Figures 6C and D illustrate the regions of hysteresis from the standpoint of current thresholds. Note in particular that the current required to attain the off-threshold increases dramatically as the calcium channel density becomes larger, even though the voltage off-threshold changes only modestly. This is due to the appreciable decrease in input resistance caused by channel opening.

6 Domains of parameter space supporting plateau and action potentials

Nonlinear systems often exhibit qualitative changes in dynamic behavior in different domains of their parameter space. Key parameters in the present model are the specific conductances of calcium and potassium channels. In previous sections, we illustrated how a qualitative change from passive responsiveness to bistable behavior with plateau potentials occurs when a certain minimum value of calcium conductance is present. We also

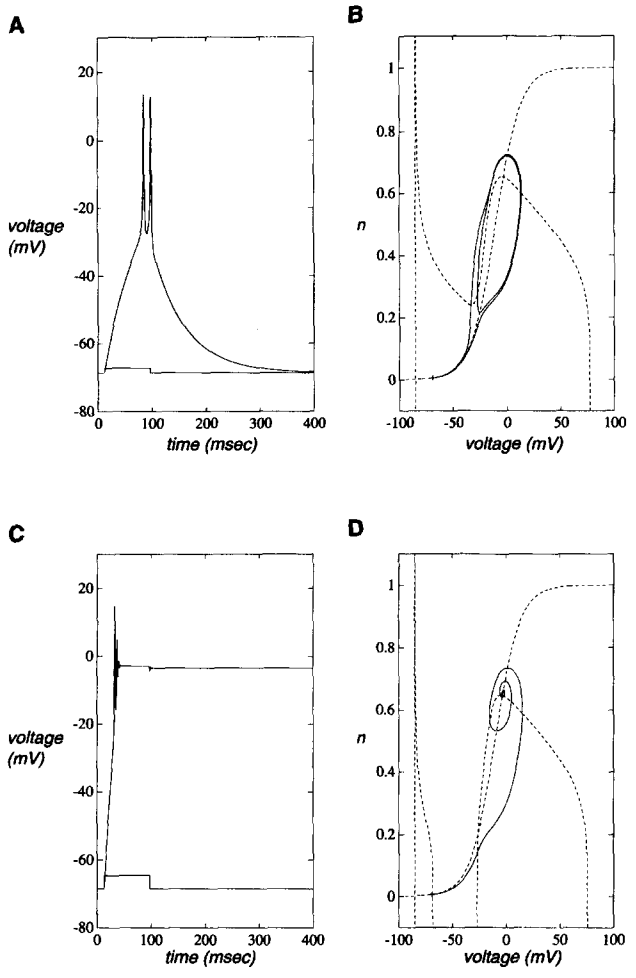

Fig. 7A–D. Calcium action potentials and plateau potential at higher conductances. In these examples, calcium and potassium conductances were set to 600 and 3120 $\mu S/cm^2$, respectively. **A** Calcium spikes were produced in response to a 1.4-nA depolarizing current pulse. **B** System nullclines in the presence of a steady 1.4-nA depolarizing current show a single equilibrium point at a depolarized potential. The phase trajectory corresponding to the time plot in **A** is shown superimposed. **C** A damped oscillation followed by a plateau potential instead was produced in response to a 4-nA depolarizing pulse. **D** System nullclines in the absence of injected current have three intersections, demonstrating a potential for bistability. The phase trajectory corresponding to the time plot in **C** is shown superimposed

illustrated how potassium conductance can counteract bistability and its hysteretic properties. Ideally, one needs to investigate the interactive effects of both calcium and potassium conductance throughout the domains of their parameter space. In this section, we explore a broader range of calcium-potassium conductance pairs, and we illustrate how high values of conductance may, within certain ranges of injected current, give rise to limit cycles and action potentials.

Figure 7 shows an example in which calcium conductance was set to 0.6 mS/cm^2, 10 times the standard value of 60 $\mu S/cm^2$ used in most of the earlier examples, and potassium conductance was set to 3.1 mS/cm^2, more than 7 times the standard value of 420 $\mu S/cm^2$. Figure 7A shows two action potentials generated in response to a 1.4-nA depolarizing pulse lasting 100 ms, and Fig. 7B shows this as a cyclical trajectory in the phase plane. In the presence of a steady 1.4-nA depolarizing current, the cyclical trajectory converged to a limit cycle that corresponded to repetitive calcium spikes in the time domain (not illustrated). When the phase of current injection terminated (e.g., when the pulse ended in Fig. 7A), the membrane consistently repolarized to its resting potential.

Qualitatively different dynamical behavior was observed with the same values of conductance when a higher intensity of depolarizing current was delivered (Fig. 7C; 4-nA pulse). Instead of repetitive action potentials, there was a rapidly damped oscillation, and the depolarization was sustained as a plateau potential after the current pulse terminated. This represents bistable behavior, as is documented by the presence of three equilibrium points in the phase-plane analysis of Fig. 7D. The voltage nullcline shown in Fig. 7D corresponds to zero injected current, so it applies to the off-responses to both 1.4-nA (Fig. 7A) and 4-nA (Fig. 7C) current pulses. It is noteworthy that the response to the smaller pulse returned to the resting equilibrium point of the system, whereas the response to the larger pulse latched at the active equilibrium point.

Similar behavior was observed in other simulations with high values of calcium and potassium conductance. Figure 8A shows a case in which a prolonged 3-nA pulse elicited repetitive action potentials, and the membrane repolarized to resting potential at the end of the pulse. A phase-plane analysis under conditions of zero injected current (not shown) revealed three equilibrium points, thus demonstrating a potential for bistable behavior. We therefore attempted to determine the conditions for reaching the upper (active) equilibrium point. The phase plane in Fig. 8B corresponds to the period during which 3 nA of current is being injected. As in cases discussed earlier, depolarizing current elevates the voltage nullcline such that there is a single equilibrium, at point *C*. When we forced the system's initial conditions to point *C* in state space, the system stayed at this stable state during the entire current pulse. In contrast, if initial conditions were set slightly away from that point, for example, at point *b* in Fig. 8B, the trajectory was repelled from point *C* and was attracted to the limit cycle shown by the heavy trajectory. This type of behavior indicates the presence of a stable limit cycle that surrounds a coexistent stable singular point, previously described by Rinzel and colleagues in a model of the squid axon (Guttman et al. 1980). Termination of the current pulse while the system is at the singular point left the system at its upper equilibrium point, as shown by trace *C* in Fig. 8A. Instead, with alternative initial conditions slightly removed from point *C*, termination of the current pulse always returned the system to its lower equilibrium point (Fig. 8A). We concluded that bistable behavior in the form of plateau potentials, while demonstrable under carefully selected conditions, was essentially unachievable in practice when g_K is high. However, in a broader context, the coexisting stable point and limit cycle are essentially a form of dynamic hysteresis which has been exploited before for

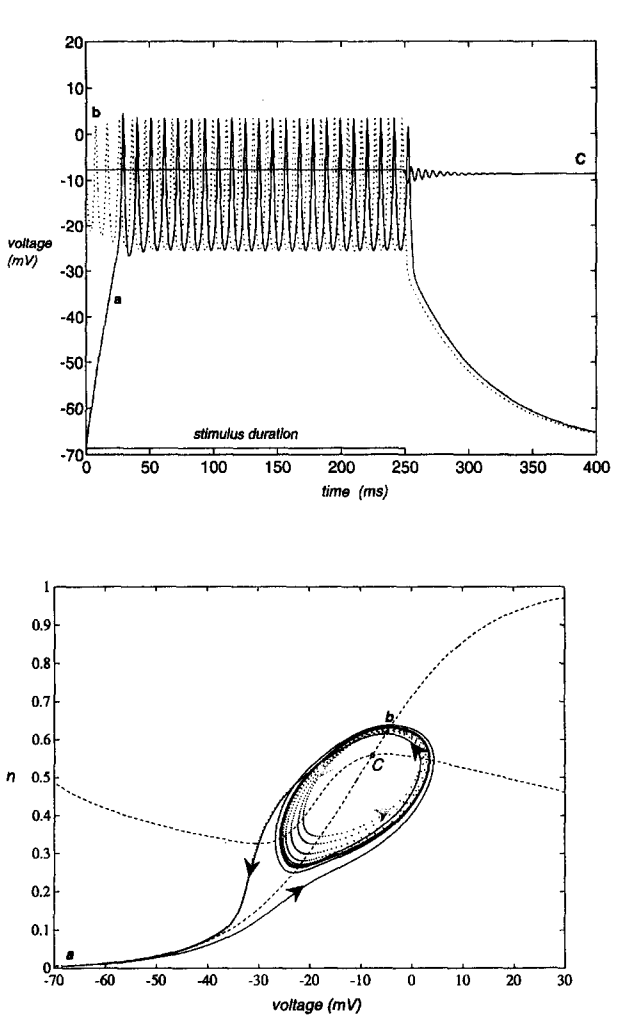

Fig. 8A, B. Co-existence of a limit cycle surrounding a stable singular point. In these examples, calcium and potassium conductances were set to 300 and 3000 $\mu S/cm^2$, respectively. Responses to current injection are shown by three time plots (**A**) and the corresponding phase trajectories (**B**). Trajectory *a* shows the response to a 250-ms depolarizing current that takes the system from rest into a stable limit cycle; the nullclines correspond to this state. However, the system remains in a constant plateau state at *C*, even when the stimulus expires, when the initial state is at this equilibrium point. In contrast, trajectory *b* shows convergence onto the limit cycle when the initial state is at point *b*

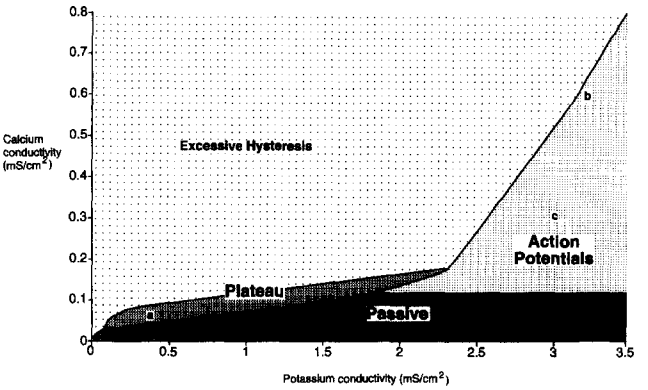

Fig. 9. Dynamic behavior of the system as a function of specific conductances. Large regions of this parameter space support plateau potentials, although only a relatively small zone near the *Passive* region has a suitable range of hysteresis to effectively support bistable operating properties. The remainder of the plateau region, labeled *Excessive Hysteresis*, requires currents in excess of 3.5 nA to produce off-state transitions. Point *a* indicates standard values of conductance as used in Figs. 2–4. Action potentials were supported at high values of potassium conductivity, provided g_{Ca} exceeded 0.1 mS/cm^2. Points *b* and *c* indicate conductances used in Fig. 7 and 8, respectively

resetting repetitive firing in squid axons (Guttman et al. 1980).

The conductance parameter space was explored systematically by running simulations with varying calcium and potassium conductances. Figure 9 summarizes the values of specific conductance that support plateau potentials, action potentials, and purely passive responses. It is clear that plateau potentials are supported by conductance pairs occupying a large fraction of this parameter space, as indicated by the checkered region. However, we wish to highlight a select portion of this space (the dark checkered region) as being the only practical region for reasonable on- and off-transitions. Included within this region are pairs of conductance values that allowed transitions with realistic amounts of injected current (< 5 nA). These on-state transitions are readily made with a variety of conductance values (Fig. 6); the more critical requirement is for reasonable off-state transitions. The latter occupy a relatively narrow range of calcium conductances (Fig. 6). Figure 9 shows how the boundaries of this range increase in parallel as potassium conductance increases. The narrowness of this calcium conductance range derives from a tradeoff between two constraints: (1) enough calcium conductance is required to produce three intersections of the nullclines (Fig. 2b), thus defining the three equilibrium points required for bistability, whereas (2) too much calcium conductance requires an unrealistically high current to make the off-state transition (Fig. 6C). Action potentials occur when potassium conductance is above about 2 mS/cm^2, and the utilization of bistability is impractical in this region.

7 Discussion

The model of a Purkinje cell dendrite analyzed in this report illustrates how bistability can arise from a relatively simple combination of voltage-gated ion channels. We have shown that a system comprised of modest concentrations of persistent calcium and delayed-rectifier potassium channels, embedded in a single-compartment electrotonic model of a dendrite, is capable of supporting bistability, hysteresis and calcium spikes. This section begins with a discussion of similarities and differences between the bistability expressed by this simplified ionic model and the plateau potentials that are observed in the dendrites of Purkinje cells. Then a comparison is made between the ionic model and the abstract model of bistability that has been used in computational studies of motor control. We will conclude that the simplified ionic model provides a useful bridge between two perspectives on bistability, a biophysical perspective that views bistability as an expression of interesting ion channels and an

integrative perspective that sees bistability as a useful computational property.

7.1 Biophysical perspective

Our model reproduces several salient features of the plateau potentials that have been recorded from Purkinje cells with intracellular and fine extracellular electrodes. Although these potentials have been recorded from both soma and dendrites, they are particularly prominent in dendrites (Llinás and Sugimori 1980a, b; Ekerot and Oscarsson 1981; Campbell et al. 1983) where their dependence on extracellular calcium ions has been demonstrated (Llinás and Sugimori 1980b). Plateau potentials can be evoked by climbing fiber stimulation (Ekerot and Oscarsson 1981), by parallel fiber stimulation (Campbell et al. 1983), or by injected current (Llinás and Sugimori 1980b), the common feature being that of depolarizing the dendritic membrane beyond a critical threshold level. When this occurs, the membrane latches into a depolarized state that can extend well beyond the duration of the stimulus.

According to our model, this threshold behavior is due to the presence of a saddle point in the phase space that describes the nonlinear dynamics of the system. A saddle point is a type of unstable equilibrium which, in the dendritic model, results from an unstable balance between an inward calcium current that tends to depolarize the dendrite further and an outward potassium current that tends to restore the membrane to its resting potential. From the standpoint of nonlinear dynamics, the saddle point B is the low point along a ridge, or watershed, that separates the $n - V$ state space of Fig. 3A into two basins of attraction. When a pulse of synaptic or injected current is sufficient to push the state of the system over this ridge, just into the upper basin, the subsequent trajectory in state space (c in Fig. 3A) descends the basin and converges onto the attractor point C. However, if the current pulse leaves the system state in the lower basin of attraction, the trajectory in state space (b in Fig. 3A) falls back to the attractor at A. Attractor C, characterizing the plateau state, corresponds to a stable balance between active inward and outward currents produced by calcium and potassium, respectively. Attractor A, characterizing the resting state, is instead dominated by leak currents that pull the membrane potential toward its resting value.

Our modeling results show that bistability is supported by a wide range of ion channel specific conductances (Sects. 5 and 6). However, when one includes additional constraints that insure plateau potentials with reasonable operating properties, the range of acceptable conductances is narrowed considerably. With calcium conductances much above 0.1 mS/cm^2, quite large hyperpolarizing currents are required to produce transitions from on-states to off-states. And with potassium conductances above about 2 mS/cm^2, transitions to on-states typically produce action potentials instead of plateau potentials. The standard values we used to generate reasonable plateau potentials (Figs. 2–4) were 60 μS/cm^2 for calcium and 420 μS/cm^2 for potassium. Assuming that the average conductance of a calcium channel is 15 pS (cf. Usowicz et al. 1992), we calculate a calcium p-channel density of 0.06 channels/μm^2. Similarly, assuming that the average conductance of a delayed-rectifier potassium channel is 60 pS (cf. Gähwiler and Llano 1989), we calculate a channel density of about 0.07 channels/μm^2. These appear to be relatively modest densities for neuronal membrane (Hille 1984, Chapter 9), although the available estimates derive from studies of axons or neurons with little dendritic membrane, so it is possible that dendrites have relatively low channel densities.

The model's plateau potentials typically reached 40–50 mV above resting potential, whereas recorded plateau potentials have an amplitude of 10–30 mV, with the largest amplitudes being observed in the most distal recordings (Llinás and Sugimori 1980b; Ekerot and Oscarsson 1981). The amplitude of a plateau potential should depend primarily on the activation thresholds of the relevant ionic conductances and on the electronic properties of the neuron. The calcium channel activation threshold used in this model (-40 mV, half-maximal at -20 mV) was based on experimental data for rats generated in our laboratory and similar values reported by Regan (1991). If one assumed higher values (cf. Usowicz et al. 1992), the discrepancy would be greater. We believe that the lower amplitudes of plateau potentials seen experimentally probably result from electrotonic attenuation. Intracellular recordings are made at best from primary or secondary dendritic branches, whereas the plateau potentials are thought to be maximal in the most distal dendritic branches, where intracellular recordings are impractical (Ekerot and Oscarsson 1981).

The transitions between plateau and action potentials in our model are interesting to compare with the results of intradendritic recordings. In our model, calcium spikes were seen only when the specific conductance of potassium channels was increased above 2 mS/cm^2. Spikes then occurred at low intensities of current injection, and increasing the current intensity often converted spiking behavior into plateau potentials. In contrast, Llinás and Sugimori (1980b, Fig. 5) found that increasing the intensity of the current injected through an intradendritic electrode caused a transition in the opposite direction; plateau potentials were converted into spiking behavior. While this might indicate a basic flaw in the model, another interpretation is that high intensities of injected current lead to an enhancement of potassium conductance. This might, for example, result from a recruitment of calcium-gated potassium channels, since depolarizing currents can produce quite substantial increases in intracellular calcium (Lev-Ram et al. 1992). The incorporation of a slow, calcium-dependent potassium conductance in future work would be most appropriate, since it might also account for the automatic resetting of plateau potentials to resting potential after plateaus of a few hundred ms.

7.2 Computational perspective

The vast majority of computational studies with neural networks have utilized units with linear, sigmoidal or

binary input-output characteristics. Bistable units have received much less attention, even though networks comprised of them have interesting additional properties (Hoffman 1986; Benson et al. 1987; Houk et al. 1990; Kiehn 1991; Wang and Ross 1990; Gutman 1991, 1994). The hysteresis inherent in bistable units amounts to a form of short-term memory that does not depend on changes in synaptic weight. This can lead to a minimization of the afferentation required to generate a motor response (Gutman 1994). Synchronous Hopfield-Tank networks using neurons with hysteresis have better memory capacity and retrieval ability in the presence of noise (Wang and Ross 1990). When used in sensorimotor networks, bistable units can convert feedback loops into quasi-feedforward pathways, and this can circumvent problems of instability that plague conventional control systems (Houk et al. 1990). Switching between on- and off-states replaces continous control in a manner that is analogous to state transitions in finite automata (Tomovic and McGhee 1966). In a recent model of the cerebellum, Purkinje cells were represented as bistable elements that learn, under the training influence of climbing fibers, the conditions for switching to their on-state (Houk et al. 1990; Houk and Barto 1992; Berthier et al. 1993). After this period of learning, Purkinje cells switch to their on-state and inhibit motor commands at appropriate times, thus terminating movements gracefully at their intended goals. This type of switching control has the potential for converting high-level planning signals into temporally patterned action commands that implement adaptive behaviors (Houk and Wise 1995).

Because networks with bistable units have these interesting computational properties, one would like to relate the abstract representation of bistability used in computational studies to the biophysical mechanisms that underlie this property. The model of a Purkinje cell dendrite presented in this report, though simplified, is a useful step in this direction. Figure 1B summarizes the steady-state properties of this ionic model in a manner that facilitates comparison with the abstract model of bistability in Fig. 1A. Both the abstract and the ionic models show discrete thresholds for state transions (vertical dashed arrows) where the output jumps discontinuously between a passive off-state and an active on-state. The main difference is that between these on- and off-thresholds, the ionic model has a graded response mediated by the physical resistance of the dendritic membrane. In contrast, the abstract model has a flat response because of the tacit assumption that membrane resistance is negligibly small. The membrane resistance of the ionic model in its on-state is much lower than in its off-state because the calcium and potassium channels are mostly open in the on-state. In order to appreciate the consequences of these finite resistances, one needs to consider how the dendritic membrane might influence the somatic membrane of a Purkinje cell, and thus produce spike discharge that could be transmitted along Purkinje axons.

The different specializations of dendritic and somatic membrane reviewed in Sect. 1 promote the notion of a model Purkinje cell with discrete dendritic and somatic compartments, separated by equivalent longitudinal resistances. A similar approach was recently proposed, and justified experimentally, for the interpretation of patch-clamp recordings from immature Purkinje cells (Llano et al. 1991). Application of this electrotonic model to adult Purkinje cells can be thought of as a reasonable approximation, and Fig. 10 shows schematically how five dendritic compartments might feed into a single somatic compartment. This model is useful in attempting to translate between the input-output properties of individual dendritic branches (Fig. 1B) and the resultant spike discharge of the Purkinje cell.

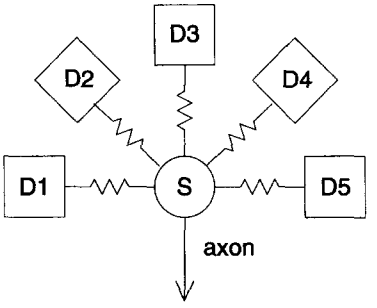

Fig. 10. Schema illustrating how five dendritic branches (*D*) of a Purkinje cell might collectively influence the soma (*S*). Bistability in each of the dendritic compartments, if sufficiently independent, would be expected to result in multistability in the cell's overall properties

Assuming a simple integrate-and-fire soma, a combined dendrite-soma model will give rise to different behavior depending on the somatic threshold for spike generation and the longitudinal resistance between the soma and dendrite. If the depolarization from the resting state of the dendrite fails to elicit any somatic spikes (spike threshold as showed by horizontal dashed line in Fig. 1B), then the output firing rate of the neuron is effectively zero, and thus one obtains a situation that is effectively approximated by the abstract model in the steady state. However, if the threshold and resistance loading are such that the soma can fire ation potentials when the dendrite is in its off-state, then effectively two windows of firing rates would be obtained from the ionic model, deviating from the abstract model in terms of the predicted firing rates. With respect to the resistance of the excited state, the values are usually low due to the opening of the channels, and therefore a zero-slope approximation is not unreasonable, as suggested by the abstract model. Thus, we conclude that under conditions of high somatic threshold for spike generation, the abstract model is a good approximation of the ionic model described here.

When more than a single dendrite is considered, the situation becomes more complex. Each dendrite can be expected to deliver to the soma a certain amount of current proportional to its membrane potential, and the currents delivered from several active dendrites would be expected to sum, though probably in a nonlinear fashion. If we assume that the state of each dendrite is determined relatively independently by its local parallel fiber inputs,

individual plateau potentials would sum at the soma. The cell as a whole should behave in a multistable fashion, although the demonstration of several stable states might be blurred by interspike interval variations. However, it may not be reasonable to assume that the individual dendrites are sufficiently isolated to behave as relatively independent current sources. These features require further assessment through modeling and appropriately designed experiments.

In this paper we have attempted to bridge the rather wide gap that currently exists between biophysical knowledge concerning the ion channels present in Purkinje cells and connectionist concepts about the computational properties of the cerebellum. The model presented of a Purkinje cell dendrite shows how an interesting computational property, namely bistability, can arise from a simple combination of voltage-gated ion channels. While the present model derives from certain assumptions about which channels and channel properties and particularly important to consider, many of the basic features of this model may apply to alternative assumptions within certain bounds. The basic properties of the model are:

1. For a range of parameter values, a saddle point exists that separates transitions between an off-state characterized by mainly passive properties of the dendritic membrane and an on-state characterized by a balance between an active inward current carried by persistent calcium channels and an active outward current carried by potassium channels. In the present model, the outward current is carried by delayed-rectifier potassium channels, but a more realistic model would have to include calcium-gated potassium channels.
2. Depolarizing currents beyond an on-threshold value produce transitions to the on-state, whereas hyperpolarizing currents beyond an off-threshold produce transitions to the off-state. The difference between on- and off-thresholds results in a region of hysteresis. Increasing the specific conductance of calcium channels widens the range of hysteresis, whereas increasing the conductance of potassium channels narrows this range. When potassium conductance is above about 2 mS/cm^2, action potentials are generated in response to modest depolarizing potentials, and transitions to plateau potentials are inhibited. The ranges of specific conductance we propose for computationally useful bistable properties may be useful in guiding experimental studies, even if alternative channels turn out to be more dominant.
3. Unlike experimentally observed plateau potentials, the plateau of the model persists indefinitely. The automatic resetting of plateaus may involve a recruitment of calcium-gated potassium currents. Alternatively, resetting might result from slow inactivation of high-threshold calcium currents. Experimental studies could resolve this question.
4. We envision that individual dendrites are capable of supporting relatively independent plateau potentials, and that the depolarization of the Purkinje cell soma would be determined by a summation (possibly nonlinear) of these individual influences. The resultant properties of the overall Purkinje cell would then be multistable. These extrapolations need to be explored both experimentally and in simulations.

Bistability has interesting computational properties that have started to attract attention in the computational literature. The present model may facilitate communication and collaboration between theorists interested in the information-processing functions of the cerebellum and experimentalists interested in the unique properties of its composite neurons.

Acknowledgements. We gratefully acknowledge the support of various aspects of this work by ONR (N-00014-93-1-0636 to G.L.Y.), NIH and NIMH (P01 NS17489 and P50 MH48185 to J.C.H.) and NIH (NS-26915 to P.E.H.).

Appendix

To examine how voltage and current thresholds depend on calcium and potassium specific conductances, we noted that the voltage derivative of the total current vanishes at the threshold for a state transition:

$$\frac{\mathrm{d}\sum I_{\mathrm{ions}}}{\mathrm{d}V} = 0 \tag{A1}$$

i.e.,

$$\frac{\mathrm{d}}{\mathrm{d}V}\left[g_{\mathrm{Ca}} s_{\mathrm{inf}}^2 (V - V_{\mathrm{Ca}}) + g_{\mathrm{K}} n^4 (V - V_{\mathrm{K}}) + g_{\mathrm{leak}} (V - V_{\mathrm{leak}})\right] = 0$$

which after differentiation becomes

$$g_{\mathrm{Ca}} s_{\mathrm{inf}}\left[s_{\mathrm{inf}} + 2\frac{\mathrm{d}s_{\mathrm{inf}}}{\mathrm{d}V}(V - V_{\mathrm{Ca}})\right] + g_{\mathrm{K}} n_{\mathrm{inf}}^3\left[n_{\mathrm{inf}} + 4\frac{\mathrm{d}n_{\mathrm{inf}}}{\mathrm{d}V}(V - V_{\mathrm{K}})\right] + g_{\mathrm{leak}} = 0 \tag{A2}$$

To visualize the effect of calcium conductance changes on the threshold voltages, g_{Ca} was expressed as a function of voltage:

$$g_{\mathrm{Ca}} = -\frac{g_{\mathrm{K}} n_{\mathrm{inf}}^3\left[n_{\mathrm{inf}} + 4\frac{\mathrm{d}n_{\mathrm{inf}}}{\mathrm{d}V}(V - V_{\mathrm{K}})\right] + g_{\mathrm{leak}}}{s_{\mathrm{inf}}\left[s_{\mathrm{inf}} + 2\frac{\mathrm{d}s_{\mathrm{inf}}}{\mathrm{d}V}(V - V_{\mathrm{Ca}})\right]} \tag{A3}$$

Analogously, using (A2) and expressing g_{K} as a function of voltage, the effect of potassium conductance change on threshold voltages can be visualized using:

$$g_{\mathrm{K}} = -\frac{g_{\mathrm{Ca}} s_{\mathrm{inf}}\left[s_{\mathrm{inf}} + 2\frac{\mathrm{d}s_{\mathrm{inf}}}{\mathrm{d}V}(V - V_{\mathrm{Ca}}) + g_{\mathrm{leak}}\right]}{n_{\mathrm{inf}}^3\left[n_{\mathrm{inf}} + 4\frac{\mathrm{d}n_{\mathrm{inf}}}{\mathrm{d}V}(V - V_{\mathrm{K}})\right]} \tag{A4}$$

Using voltage as the independent variable in either (A3) or (A4) and computing the corresponding maximum conductance value allows one to visualize the dependence of the threshold voltage on the conductances (Fig. 6A, B). The corresponding current thresholds (Fig. 6C, D) were evaluated from (5), using the above values of voltage threshold and conductance to compute the corresponding steady-state ionic currents.

References

Anderson JA, Rosenfeld E (1988) Neurocomputing: foundations of research. MIT Press, Cambridge, Mass.

Andersson G, Campbell NC, Ekerot C-F, Hesslow G, Oscarsson O (1984) Integration of mossy fiber and climbing fiber inputs to Purkinje cells. Exp Brain Res (Suppl) 9:145–150

Benson MW, Bree GM, Kinahan PE, Hoffmann GW (1987) A teachable neural network based on an unorthodox neuron. Physica D 22:233–246

Berthier NE, Singh SR, Barto AG, Houk JC (1993) Distributed representation of limb motor programs in arrays of adjustable pattern generators. J Cogn Neurosci 5:56–78

Bush PC, Sejnowski TJ (1991) Simulations of a reconstructed cerebellar Purkinje cell based on simplified channel kinetics. Neural Comput 3:321–332

Campbell NC, Ekerot C-F, Hesslow G, Oscarsson O (1983) Dendritic plateau potentials evoked in Purkinje cells by parallel fibre volleys in the cat. J Physiol (Lond) 340:209–223

Ekerot C-F, Oscarsson O (1981) Prolonged depolarization elicited in Purkinje cell dendrites by climbing fiber impulses in the cat. J Physiol (Lond) 318:207–221

Fitzhugh R (1959) Thresholds and plateaus in the Hodgkin-Huxley nerve equations. J Gen Physiol 43:867–896

Gähwiler BH, Llano I (1989) Sodium and potassium conductances in somatic membranes of rat Purkinje cells from organotypic cerebellar cultures. J Physiol (Lond) 417:105–122

Gear CW (1971) Numerical initial value problems in ordinary differential equations. Prentice-Hall, Englewood Cliffs

Gutman AM (1991) Bistability of dendrites. Int J Neural Sys 1:291–304

Gutman AM (1994) Gelfand-Tsetlin principle of minimal afferentation and bistability of dendrites. Int J Neural Syst 5:83–86

Guttman R, Lewis S, Rinzel J (1980) Control of repetitive firing in squid axon membrane as a model for a neuroneoscillator. J Physiol (Lond) 305:377–395

Hille B (1984) Ionic channels of excitable membranes. Sinauer Associates, Sunderland

Hockberger PE, Nam SC (1994) High-voltage-activated calcium current in developing neurons is insensitive to nifedipine. Pflugers Arch 426:402–411

Hodgkin AL, Huxley AF (1952) A quantitative description of membrane current and its application to conduction and excitation in nerve. J Physiol (Lond) 117:500–544

Hoffmann GW (1986) A neural network model based on the analogy with the immune system. J Theor Biol 122:33–67

Hopfield JJ, Tank DW (1986) Computing with neural circuits: a model. Science 233:625–633

Houk JC, Barto AG (1992) Distributed sensorimotor learning. In: Stelmach GE, Requin J (eds) Tutorials in motor behavior II. Elsevier, Amsterdam, pp 71–100

Houk JC, Wise SP (1995) Distributed modular architectures linking basal ganglia, cerebellum and cerebral cortex: their role in planning and controlling action. Cerebral Cortex 5:95–110

Houk JC, Singh SP, Fisher C, Barto AG (1990) An adaptive sensorimotor network inspired by the anatomy and physiology of the cerebellum. In: Miller WT, Sutton RS, Werbos PJ (eds) Neural networks for control. MIT Press, Cambridge, Mass, pp 301–348

Kiehn O (1991) Plateau potentials and active integration in the 'final common pathway' for motor behaviour. Trends Neuro Sci 14:68–73

Knight BW (1972) The relationship between the firing rate of a single neuron and the level of activity in a population of neurons. J Gen Physiol 59:767–778

Larson-Prior LJ, McCrimmon DR, Slater NT (1990) Slow excitatory amino acid receptor-mediated synaptic transmission in turtle cerebellar Purkinje cells. J Neurophysiol 63:637–650

Lasser-Ross N, Ross WN (1992) Imaging voltage and synaptically activated sodium transients in cerebellar Purkinje cells. Proc R Soc Lond Biol 247:35–39

Lev-Ram V, Miyakawa H, Lasser-Ross N, Ross WN (1992) Calcium transients in cerebellar Purkinje neurons evoked by intracellular stimulation. J Neurophysiol 68:1167–1177

Llano I, Marty A, Armstrong CM, Konnerth A (1991) Synaptic- and agonist-induced excitatory currents of Purkinje cells in rat cerebellar slices. J Physiol (Lond) 434:183–213

Llinás R, Sugimori M (1980a) Electrophysiological properties of in vitro Purkinje cell somata in mammalian cerebellar slices. J Physiol (Lond) 305:171–195

Llinás R, Sugimori M (1980b) Electrophysiological properties of in vitro Purkinje cell dendrites in mammalian cerebellar slices. J Physiol (Lond) 305:197–213

Mascagni MV (1989) Numerical methods for neuronal modeling. In: Koch C, Segev I (eds) Methods in neuronal modeling. MIT Press, Cambridge, Mass, pp 439–484

Minsky ML, Papert SA (1969) Perceptrons. MIT Press, Cambridge, Mass.

Mintz IM, Adams ME, Bean BP (1992) P-type calcium channels in rat central and peripheral neurons. Neuron 9:85–95

Morris C, Lecar H (1981) Voltage oscillations in the barnacle giant muscle fiber. Biophys J 35:193–213

Pellionisz A, Llinás R (1977) A computer model of cerebellar Purkinje cells. Neuroscience 2:37–48

Rapp M, Yarom Y, Segev I (1992) The impact of parallel fiber background activity on the cable properties of cerebellar Purkinje cells. Neural Comput 4:518–533

Regan LJ (1991) Voltage-dependent calcium currents in Purkinje cells from rat cerebellar vermis. J Neurosci 11:2259–2269

Rinzel J, Ermentrout GB (1989) Analysis of neural excitability and oscillations. In: Koch C, Segev I (eds) Methods in neuronal modeling. MIT Press, Cambridge, Mass., pp 135–169

Rose RM, Hindmarsh JL (1985) A model of a thalamic neuron. Proc R Soc Lond [Biol] 225:161–193

Ross WN, Werman R (1987) Mapping calcium transients in the dendrites of Purkinje cells from guinea-pig cerebellum in vitro J Physiol (Lond) 389:319–336

Rumelhart DE, McClelland JL (1986) Parallel distributed processing: explorations in the microstructure of cognition. Bradford Books/ MIT Press, Cambridge, Mass.

Schutter de E, Bower J (1994) An active membrane model of the cerebellar Purkinje cell. J Neurophysiol 71:375–419

Shelton DP (1985) Membrane resistivity estimated for the Purkinje neuron by means of a passive computer model. Neuroscience 14: 111–131

Sinkjaer T, Wu CH, Barto A, Houk JC (1990) Cerebellum control of endpoint position – a simulation model. IJCNN 90 II:705–710

Tank DW, Sugimori M, Connor JA, Llinás RR (1988) Spatially resolved calcium dynamics of mammalian Purkinje cells in cerebellar slice. Science 242:773–777

Tomovic R, McGhee RB (1966) A finite state approach to the synthesis of bioengineering control systems. IEEE Trans HFE-7:65–69

Usowicz MM, Sugimori M, Cherksey B, Llinás R (1992) P-type calcium channels in the somata and dendrites of adult cerebellar Purkinje cells. Neuron 9:1185–1199

Wang L, Ross J (1990) Synchronous neural networks of nonlinear threshold elements with hysteresis. Proc Natl Acad Sci USA 87:988–992

Yool AJ, Dionne VE, Groul DL (1988) Developmental changes in K selective channel activity during differentiation of the Purkinje neurone in culture. J Neurosci 8:1971–1980

Yuen GL, Hockberger PE, Massone LE, Houk JC (1992) Qualitative dynamical model of bistability in Purkinje cell dendrites. Abstr Soc Neurosci 18:1206